chlorine atom protruding outside the film surface (as shown at the top of Fig. 4). The same conclusion could be obtained in a wide spatial region from the study of ordinary Penning ionization electron spectroscopy, which also showed[16] the change in the molecular orientation during layer-by-layer deposition of ClAlPc on graphite. In Fig. 4 the spectrum of the ClAlPc island (circles) is a mixture of the monolayer spectrum (black dots) and the Grafoil spectrum (Fig. 3*b*), indicating the diffusion of molecules of the ClAlPc island on Grafoil. Thus the spectrum obtained by MEEM probes the molecular diffusion in the monolayer, as well as the orientation of molecules at the outermost surface layer with high spatial resolution.

Emission spectromicroscopy, using metastable atoms as probes, provides information on the distribution of individual orbitals exposed outside the outermost layer of the surface. There are other electron spectroscopies (such as ultraviolet photoelectron spectroscopy, X-ray photoelectron spectroscopy and electron energy-loss spectroscopy) that allow detailed analyses of the structure and electronic state of the surface. These other methods, however, give information on the outermost surface layer mixed with that on inner layers, because photons and electrons used as probes penetrate below the surface. Metastable-atom electron spectroscopy is free from such an effect and provides direct information on the outermost layer, although the quantitative analysis of the data is rather difficult because of its complex ionization mechanism. Furthermore, metastable atoms with thermal kinetic energy are essentially non-destructive (in fact, LEEM gave no sign of ClAlPc for monolayers on graphite owing to electron sputtering). The present technique, therefore, is suitable for the observation of more chemically fragile surfaces such as organic layers and biological specimens. □

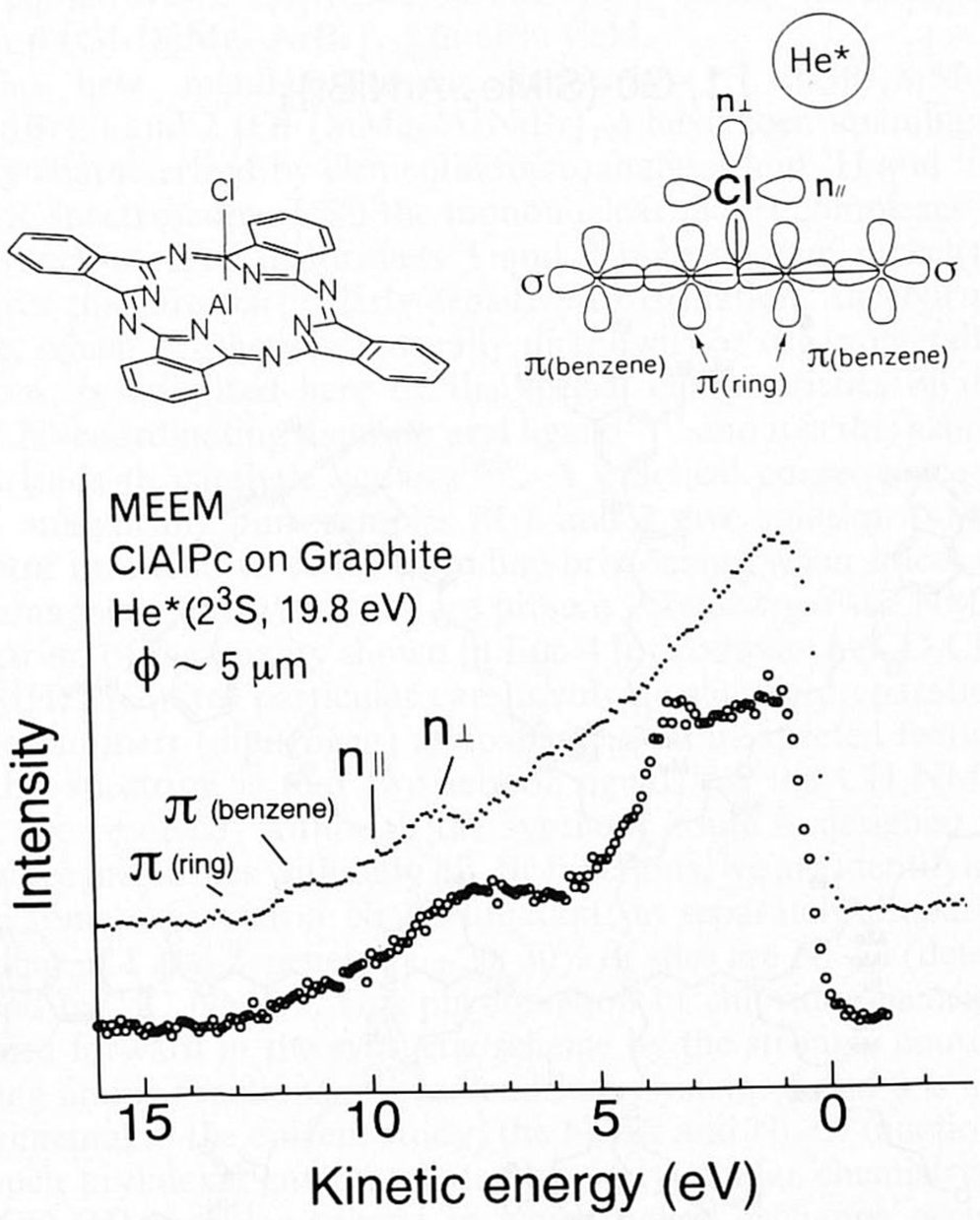


FIG. 4 Bottom, metastable electron emission spectra of a ClAlPc monolayer (black dots) and a ClAlPc monolayer island (circles) on Grafoil. Both spectra were measured 3 h after vacuum deposition of the sample. Top, schematic diagram showing the interaction between a He* metastable atom and molecular orbitals of ClAlPc. The $\pi$(ring) orbitals are distributed along the CN skeleton of the inner porphine-like ring, whereas $\pi$(benzene) orbitals are predominantly distributed in the benzene rings[17,18]. The Cl($n_{\parallel}$) and Cl($n_{\perp}$) orbitals are the chlorine lone-pair orbitals distributed parallel and perpendicular to the phthalocyanine ring, respectively. In the monolayer, molecules are oriented flat to the substrate with the chlorine atom protruding outside, because He* atoms effectively interact with the Cl($n_{\parallel}$), Cl($n_{\perp}$) and $\pi$(benzene) orbitals giving stronger bands in the spectrum, while the $\pi$(ring) and $\sigma$ orbitals (shielded by the Cl and the $\pi$(benzene) orbitals) show weaker bands.

Received 31 May; accepted 9 November 1994.

1. Turner, D. W. *Chem. in Britain* **25,** 797–800 (1989).
2. Griffith, O. H., Habliston, P. A. & Birrel, G. B. *Ultramicroscopy* **36,** 262–274 (1991).
3. Munakata, T., Ishikawa, E., Kinoshita, I. & Kasuya, T. *Rev. Sci. Instrum.* **62,** 2572–2578 (1991).
4. Conrad, H., Ertl, G., Küppers, J. & Wang, S. W. *Phys. Rev. Lett.* **42,** 1082–1086 (1979).
5. Munakata, T., Ohno, K. & Harada, Y. *J. chem. Phys.* **72,** 2880–2881 (1980).
6. Plummer, I. R. *et al. Nature* **303,** 599–601 (1983).
7. Hagstrum, H. D. *Phys. Rev. Lett.* **43,** 1050–1053 (1979).
8. Harada, Y. & Ozaki, H. *Jap. J. appl. Phys.* **26,** 1201–1214 (1987).
9. Ohno, K. & Harada, Y. in *Theoretical Models of Chemical Bonding* (ed. Maksic, Z. B.) Part 3 (Springer, Berlin, 1991).
10. Swan, A., Marynowski, M., Franzen, W., El-Batanouny, M. & Martini, K. M. *Phys. Rev. Lett.* **71,** 1250–1253 (1993).
11. Telieps, W. & Bauer, E. *Ultramicroscopy* **17,** 57–66 (1985).
12. Leasure, E. L., Mueller, C. R. & Ridley, T. Y. *Rev. Sci. Instrum.* **46,** 635–637 (1975).
13. Fahey, D. W., Parks, W. F. & Schearer, L. D. *J. Phys.* **E13,** 381–383 (1980).
14. Masuda, S., Hayashi, H. & Harada, Y. *Phys. Rev.* B**42,** 3582–3585 (1990).
15. Masuda, S., Hayashi, H. & Harada, Y. *J. Electron Spectrosc. Relat. Phenom.* **51,** 167–171 (1990).
16. Pasinszki, T. *et al. J. phys. Chem.* (submitted).
17. Höchst, H., Goldmann, A., Hüfner, S. & Malter, H. *Phys. Status Solidi* B**76,** 559–568 (1976).
18. Battye, F. L., Goldmann, A. & Kasper, L. *Phys. Status Solidi* B**80,** 425–432 (1977).

ACKNOWLEDGEMENTS. We thank N. Ueno for helpful discussions, and H. Itoh, K. Haneishi, H. Yasufuku and K. Sanpei for their technical help. This work was supported by a Grant-in-Aid for Specially Promoted Research from the Ministry of Education, Science and Culture, Japan.

# Homogeneous catalysts based on silane dendrimers functionalized with arylnickel(II) complexes

**Joan W. J. Knapen*, Alexander W. van der Made†, Janine C. de Wilde†, Piet W. N. M. van Leeuwen†‡, Peter Wijkens*, David M. Grove* & Gerard van Koten*§**

* Debye Institute, Department of Metal-Mediated Synthesis, Utrecht University, Padualaan 8, 3584 CH Utrecht, The Netherlands
† Koninklijke/Shell-Laboratorium, Amsterdam, (Shell Research BV) PO Box 3800, 1030 BN, The Netherlands

**AT the interface between heterogeneous and homogeneous catalysis there is great scope for the development of new materials that combine the advantages and/or minimize disadvantages associated with each of these classes. In particular there is a need for homogeneous catalysts with properties that allow their ready removal from a product-containing solution. One approach to such materials is to anchor homogeneous catalysts to soluble polymer supports[1]; we have recently prepared such catalytic materials in which the active centre is an organometallic species[2,3]. One disadvantage encountered when anchoring catalytic metal sites to polymers is the difficulty of accurate control of the number and location of these sites. Here we report an alternative approach—the synthesis of polysilane dendrimers (highly branched macromolecules[4–6]) which are functionalized at their periphery with metal-containing catalytically active sites. These dendrimers show regiospecific catalytic activity for the Kharasch addition of polyhalogenoalkanes to carbon–carbon double bonds. It should be possible to remove the nanoscale catalytic macromolecules of this type from the solution of products using filtration methods.**

‡ Present address: Van't Hoff Research Institute, Inorganic Chemistry and Homogeneous Catalysis, Nieuwe Achtergracht 166, 1018 WV Amsterdam, The Netherlands.
§ To whom correspondence should be addressed.

Recent advances with the incorporation of inorganic (metal) functionalities in dendrimers have included the synthesis of dendrimeric complexes with organoplatinum(IV) units[7] and ruthenium(II) coordination centres[8], as well as of some highly branched macromolecules with iron[9] and ruthenium organometallic centres[10,11]. In a previous report[5], it was intimated that a dendrimer architecture might offer a means of better controlling the disposition of pendant metal-containing catalytic sites in soluble, polymer-based catalysts.

Our target molecules in this investigation are two organometallic polysilane dendrimers functionalized with four (**1**, generation 0; G0-$\{SiMe_2\text{-}ArNiBr\}_4$; $M_r = 2{,}269$; Fig. 1*a*) and twelve (**2**, generation 1; G1-$\{SiMe_2\text{-}ArNiBr\}_{12}$; $M_r = 7{,}032$; Fig. 1*b*) diamino arylnickel(II) complexes on their periphery. The peripheral organometallic site, like that in diamino arylnickel(II) complexes **3** (Fig. 2), is one in which the metal centre is fixed by a metal–carbon $\sigma$-bond to the ligand system. This site has been shown, both in mononuclear complexes such as **3** (ref. 12) and when anchored in soluble siloxane polymers[3], to be particularly effective for homogeneous catalysis of the Kharasch addition reaction of polyhalogenoalkanes to an olefinic C=C double bond:

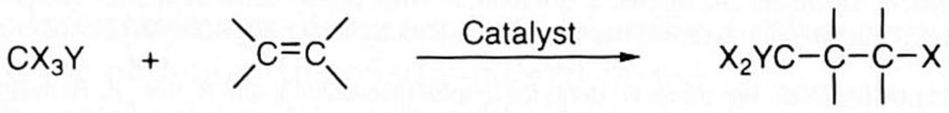


Here X denotes a halogen, and Y denotes either H, halogen, $CF_3$ or other electronegative group. The alkenes used were, for example, methyl methacrylate, 1-octene and styrene. An attractive property of catalysts such as **3** is that they selectively produce the 1:1 adduct: that is, oligomeric or polymeric products are essentially absent.

The divergent synthetic route to the catalytic dendrimers **1** and **2**, outlined in Fig. 3, begins with the silane $Si(CH_2CH{=}CH_2)_4$ (generation 0; G0) and the silane dendrimer $Si\{CH_2CH_2CH_2\text{-}Si(CH_2CH{=}CH_2)_3\}_4$ (generation 1;

*a*

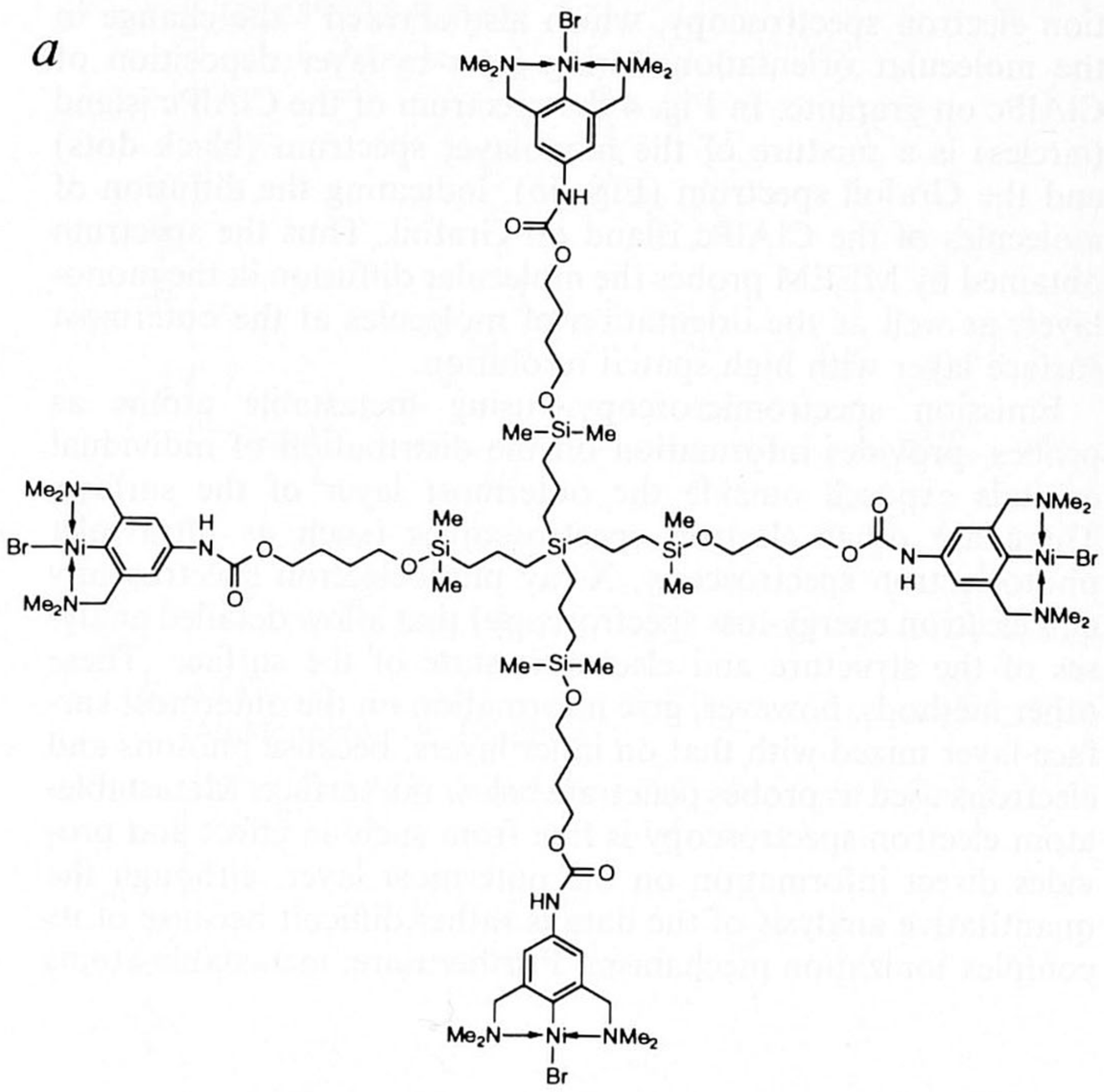


**1**, G0-$\{SiMe_2\text{-}ArNiBr\}_4$

*b*

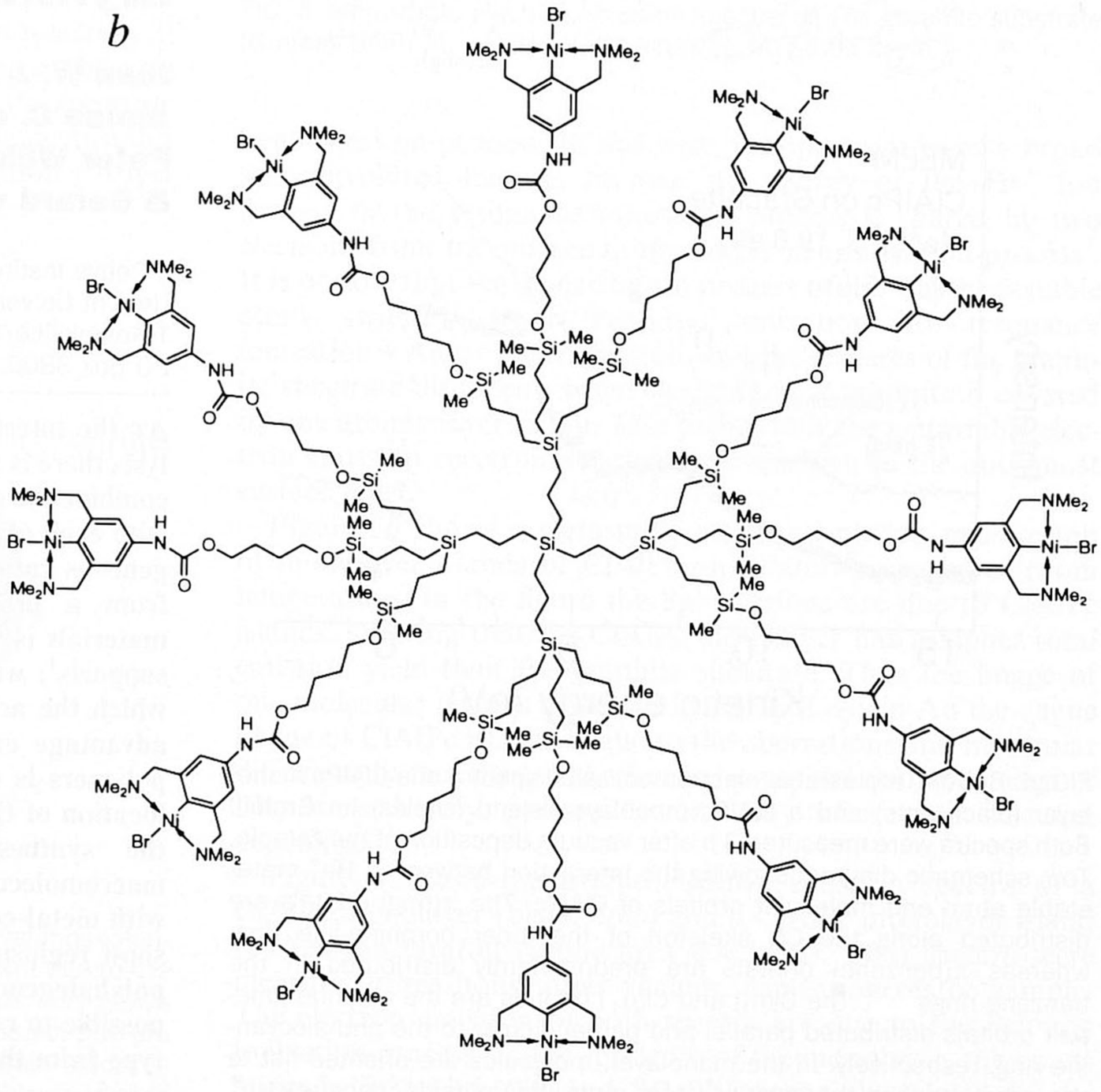


**2**, G1-$\{SiMe_2\text{-}ArNiBr\}_{12}$

FIG. 1 Schematic structures of the functionalized dendrimer catalysts. *a*, **1**, G0-$\{SiMe_2\text{-}ArNiBr\}_4$; *b*, **2**, G1-$\{SiMe_2\text{-}ArNiBr\}_{12}$.

G1) for which syntheses have been reported earlier by us[13,14] and by others[15]. These silanes were converted with $HSiClMe_2$ to the corresponding $SiMe_2Cl$ derivatives in which the number of Si–Cl functional groups is restricted to four (G0-$\{SiMe_2Cl\}_4$) and twelve (G1-$\{SiMe_2Cl\}_{12}$), respectively. In the next stage a diamino aryl bromide, the precursor entity for the organometallic site, was connected to the periphery of G0-$\{SiMe_2Cl\}_4$ and Gl-$\{SiMe_2Cl\}_{12}$ by a 1,4-butanediol linker. To achieve this the 4-amino-substituted 2,6-bis[(dimethylamino)methyl]-1-bromobenzene, **4b** (ref. 2) was first reacted with triphosgene to afford the isocyanate derivative **4c** as its dihydrogenchloride salt[16]. This was subsequently converted with excess 1,4-butanediol (45 °C, 3 h) to the alcohol **4d**. Reaction of one mol-equivalent of G0-$\{SiMe_2Cl\}_4$ with four mol-equivalents of **4d** in the presence of triethylamine afforded the dendrimer system **5** (G0-$\{SiMe_2$-ArBr$\}_4$, Fig. 3) with a peripheral aryl bromide unit that was isolated in 81% yield after washing the reaction mixture with aqueous base and removing all volatiles *in vacuo*. In a similar way, starting from Gl-$\{SiMe_2Cl\}_{12}$ and **4d**, the aryl bromide substituted dendrimer **6** (Gl-$\{SiMe_2$-ArBr$\}_{12}$, Fig. 3) was obtained in 67% yield.

We found, based on earlier studies[3], that dendrimer **5** reacts with excess zerovalent nickel complex $Ni(PPh_3)_4$ in tetrahydrofuran (THF) for 4 h at 60–70 °C to produce the desired oxidative addition product **1**, G0-$\{SiMe_2$-ArNiBr$\}_4$, (Fig. 1*a*). The crude product was separated from excess $Ni(PPh_3)_4$ and free $PPh_3$ by several precipitations from benzene and THF solutions with either hexane or ether to give **1** as an orange solid in 58% yield. In a similar way **2**, Gl-$\{SiMe_2$-ArNiBr$\}_{12}$ (Fig. 1*b*) was obtained from **6** (Gl-$\{SiMe_2$-ArBr$\}_{12}$) in 60% yield.

The new metal-containing dendrimers **1** (G0-$\{SiMe_2$-ArNiBr$\}_4$) and **2** (Gl-$\{SiMe_2$-ArNiBr$\}_{12}$) have been unambiguously characterized by elemental microanalyses and $^1H$ and $^{13}C$ NMR spectroscopy. Like the mononuclear nickel complexes **3**, the functionalized dendrimers **1** and **2** both contain nickel(II) centres that are particularly sensitive to oxidation; the Ni(III) state, which is otherwise virtually unknown for organometallic species, is stabilized here by the special characteristics of the N,C,N′-coordinating diamino aryl ligand[17,18] and it is this aspect that leads to catalytic activity[19,20]. A practical consequence is that analytically pure samples of **1** and **2** give solution NMR spectra that tend to suffer from line-broadening when traces of paramagnetic Ni(III) centres are present; obtaining a $^{13}C$ NMR spectrum of the quality shown in Fig. 4 for complex **1** ($CD_2Cl_2$, 75 MHz) requires particular care involving sample preparation under an inert (dinitrogen) atmosphere. An unexpected feature of this spectrum is that two sets of signals for the $CH_2NMe_2$ unit are resolved. Although the synthetic route is designed to produce metal sites with only Ni–Br functions, we are identifying here some sites with a Ni–Cl function; in separately prepared batches of **1** and **2**, generally ~20–30% of sites are Ni–Cl (determined by $^{13}C$ NMR). This phenomenon of chloride ion being carried forward in the synthetic scheme by the strongly coordinating amine functions of our dendrimer systems **5** and **6** is not detrimental in the current study; the Ni–Br and Ni–Cl functions in such arylnickel environments have very similar chemistry[19]. In $CD_3OD$, a polar solvent in which halide exchange occurs easily, the $^1H$ and $^{13}C$ NMR spectra of **1** give a single resonance pattern for the $-C_6H_2(CH_2NMe_2)_2$-2,6 groupings consistent with the presence of only one type of metal site.

Fast-atom-bombardment (FAB) mass spectrometric analysis of **1** (methanol solution added to a monothioglycerol or mNBA (*m*-nitrobenzyl alcohol) matrix affords spectra containing many ion clusters all having complex isotope patterns that, at this stage, are not suitable for assuring the fidelity of the proposed structure. We assume that the complexity results from the oxidation sensitivity of **1** in solution in combination with interactions with the matrices used and the presence of bromide and chloride in the sample. We are searching for the most appropriate procedures and techniques for acquiring representative mass spectral data of multinuclear dendrimeric species **1** and **2**, as well as of mononuclear complexes **3**, so that in future research mass spectrometry can be used as a tool for identifying and characterizing such dendrimeric organometallic molecules.

TABLE 1 Catalytic activity of mononuclear complex **3a** and the dendrimers **1**, **2**

| Complex | Number of Ni sites (mol × $10^{-5}$) | Reaction time (h) | Conversion* (%) | Initial reaction rate† (turnovers per Ni site per h) |
|---|---|---|---|---|
| **3a** | 10.06 | 0.25 | 21 | 234 |
| | 10.06 | 2 | 80 | — |
| **1**, G0-$\{SiMe_2$-ArNiBr$\}_4$ | 10.01 | 0.25 | 17 | 190 |
| | 10.01 | 2 | 74 | — |
| **2**, G1-$\{SiMe_2$-ArNiBr$\}_{12}$ | 9.4 | 0.25 | 14 | 167 |
| | 9.4 | 2 | 63 | — |

Reaction conditions: to a solution of methyl methacrylate (2.8 g, 28.0 mmol), $CCl_4$ (10.0 ml, 104 mmol) and *n*-dodecane as internal gas chromatography (GC) standard (2.0 ml) in $CH_2Cl_2$ (12 ml) at 25 °C, a solution was added of catalytic complex (33.2 mg **3a**; 56.8 mg **1**; 55.2 mg **2**) in $CH_2Cl_2$ (2 ml).

* Selectivity for the formation of the 1:1 adduct of methyl methacrylate with $CCl_4$ is 100%. Conversion calculated from formation of the 1:1 adduct as determined by GC analysis.

† During the first 15 min.

The dendrimers **1** and **2** have been successfully employed as homogeneous catalysts for the Kharasch addition reaction. Under standard reaction conditions (room temperature, $CH_2Cl_2$ as solvent) using methyl methacrylate as substrate with $CCl_4$ as reagent, the catalytic activity of these two dendrimers as shown by kinetic data (Table 1) is 20% and 30% less, respectively, than that of the monomeric organometallic complex **3a** (initial rate ±234 turnovers per metal site per hour). This similarity in reactivity magnitude was expected; molecular models of the two dendrimers show the nickel sites to be well separated from one another at the end of long flexible branches and consequently the accessibility of the catalytically active nickel centre should be similar to that in **3a**. In separate kinetic studies using derivatives of **3a** we have established that the electron-withdrawing *para*-substituent –NHC(O)Oalkyl has a small positive effect on the catalytic activity compared to H, (unsubstituted **3a**)[2]. In the dendrimeric catalytic system all characteristics found for the monomeric model are retained. That is, there is clean regiospecific formation of the 1:1 addition product without polymerization of the alkene or production of $C_2Cl_6$ from $CCl_3$ radical dimerization.

Thus the new dendrimers **1** (G0-$\{SiMe_2$-ArNiBr$\}_4$) and **2** (Gl-$\{SiMe_2$-ArNiBr$\}_{12}$), represent nanoscopic catalysts with physical characteristics such as size, solubility and dispersity of catalytic sites that—unlike those in related systems with conventional polymers[3]—are very precisely defined, so affording these molecules advantageous properties for physical separation and catalyst recycling. The divergent synthesis employed for zero- and

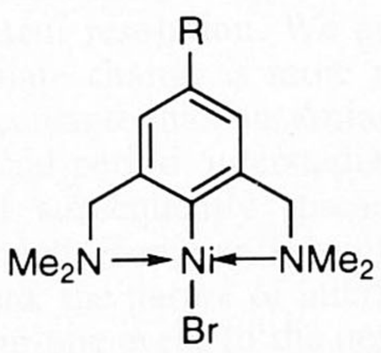


**3a**, R = H
**3b**, R = $NH_2$

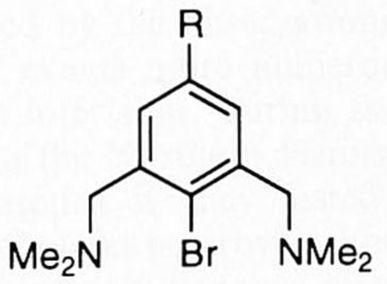


**4a**, R = H
**4b**, R = $NH_2$
**4c**, R = N=C=O
**4d**, R = $NHCO_2(CH_2)_4OH$

FIG. 2 Mononuclear arylnickel(II) complexes **3** and aryl bromides **4**.

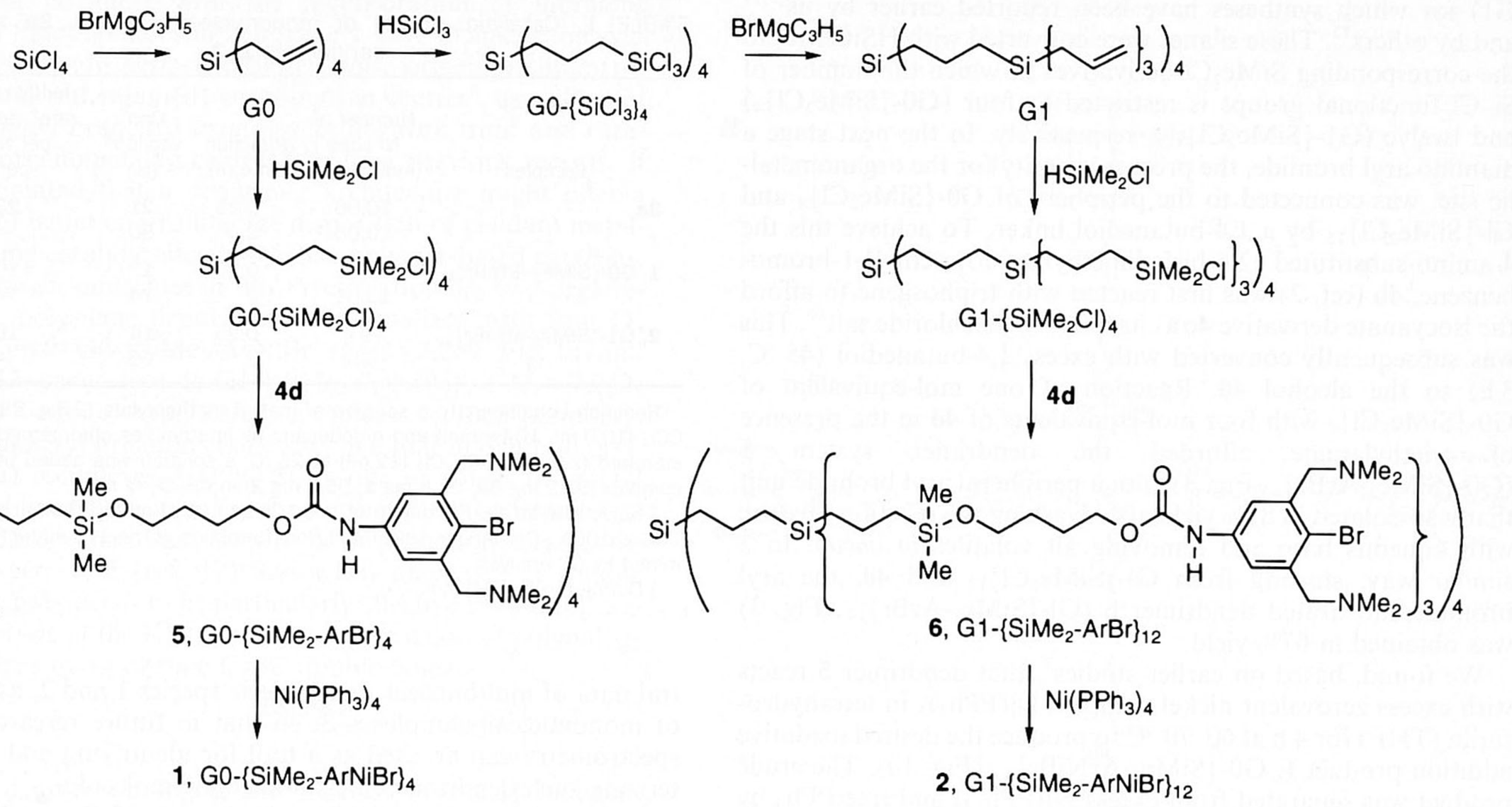


FIG. 3 Divergent synthesis of various functionalized silane dendrimers. Specific reaction conditions: **4d**, with $CH_2Cl_2$, $NEt_3$, 20 min reflux; Ni $(PPh_3)_4$, with THF, 60–70 °C, 4h. Selected physical data for **1**, G0-{$SiMe_2$-ArNiBr}$_4$: $^1$H NMR (300 MHz, $CD_2Cl_2$); chemical shift $\delta$ 6.82 (br s, 4 H, N*H*), 6.71 (s, 8 H, aryl), 4.10 (t, $J$ = 6.4 Hz, 8 H, $CO_2CH_2$), 3.61 (s, 16 H, $CH_2N$), 3.59 (t, $J$ = 6.0 Hz, 8 H, $CH_2OSi$), 2.63 and 2.68 (2 × s, 48 H, $NMe_2$), 1.68 (m, 8 H, $CH_2CH_2OSi$), 1.57 (m, 8 H, $CO_2CH_2CH_2$), 1.39 (m, 8 H, $SiCH_2CH_2$), 0.66 (t, $J$ = 8.1 Hz, 8 H, $OSi(Me)_2CH_2$), 0.60 (t, $J$ = 8.1 Hz, 8 H, $Si(CH_2)_4$), 0.07 (s, 24 H, $OSi(CH_3)_2$). $^{13}$C NMR (75 MHz, $CD_2Cl_2$); $\delta$ 154.16 (4 C, $NHCO_2$), 147.03 (8 C, aryl), 144.75 (4 C, aryl) 136.07 (4 C, aryl) 110.01 (8 C, aryl), 73.67 and 73.97 (8 C, $CH_2N$), 65.24 (4 C, $CO_2CH_2$), 62.39 (4 C, $CH_2OSi$), 51.39 and 52.25 (16 C, $NMe_2$), 29.45 (4 C, $CH_2CH_2OSi$) 26.01 (4 C, $CO_2CH_2CH_2$), 21.52 (4 C, $CH_2SiO$), 18.28 (4 C, $SiCH_2CH_2$), 17.51 (4 C, Si $(CH_2)_4$), −1.94 (8 C, $SiMe_2$). ($J$, homo- or heteronuclear spin–spin coupling constant; s, singlet; t, triplet; m, multiplet and br, broad.) Infrared; $\nu_{max}$ 3,280 (NH), 1,724 (C=O), 1,530 (NH), 1,225 (C–O) cm$^{-1}$. Elemental microanalysis: calculated for $C_{88}H_{156}Br_4N_{12}Ni_4O_{12}Si_5$; C, 46.58; H, 6.93; N, 7.41 Ni, 10.34; found; C, 46.76; H, 7.20; N, 7.37 Ni, 10.40%. Selected physical data for **2**, G1-{$SiMe_2$-ArNiBr}$_{12}$: $^1$H NMR (300 MHz, $CD_2Cl_2$); $\delta$ 6.98 (br s, 12 H, N*H*), 6.68 (s, 24 H, aryl), 4.10 (t, $J$ = 6.3 Hz, 24 H, $CO_2CH_2$), 3.66 (br s, 48 H, $CH_2N$), 3.59 (t, $J$ = 6.0 Hz, 24 H, $CH_2OSi$), 2.71 (s, 48 H, $NMe_2$), 1.67 (m, 24 H, $CH_2CH_2OSi$), 1.59 (m, 24 H, $CO_2CH_2CH_2$), 1.38 (m, 32 H, $SiCH_2CH_2$), 0.67 (t, $J$ = 8.0 Hz, 24 H, $OSi(Me)_2CH_2$), 0.60 (t, $J$ = 8.1 Hz, 40 H, $Si(CH_2)_4$), 0.08 (s, 72 H, $OSi(CH_3)_2$). $^{13}$C NMR (75 MHz, $CD_2Cl_2$); $\delta$ 154.29 (12 C, $NHCO_2$), 148.2 (br, 36 C, aryl), 136.3 (br, 12 C, aryl), 109.6 (24 C, aryl), 73.2 (br, 24 C, $CH_2N$), 65.20 (12 C, $CO_2CH_2$), 62.44 (12 C, $CH_2OH$), 52.35 (br, 48 C, $NMe_2$), 29.48 (12 C, $CH_2CH_2OSi$), 26.03 (12 C, $CO_2CH_2CH_2$), 21.57 (12 C, $CH_2SiO$), 19.06 (4 C, $CH_2SiCH_2CH_2CH_2SiCH_2$), 18.35 (12 C + 8 C, $OSiCH_2CH_2 + CH_2SiCH_2CH_2CH_2SiCH_2$), 17.59 (12 C, $Si(CH_2CH_2CH_2Si)_4$), −1.78 (24 C, $SiMe_2$). Infrared; $\nu_{max}$ 3,280 (NH), 1,725 (C=O), 1,530 (NH), 1,225 (C–O) cm$^{-1}$. Elemental microanalysis: calculated for $C_{276}H_{492}Br_{12}Ni_{12}N_{36}O_{36}Si_{17}$; C, 47.15; H, 7.05; N, 7.17; Ni, 10.01: found; C, 47.08; H, 7.10; N, 7.12; Ni, 10.10%.

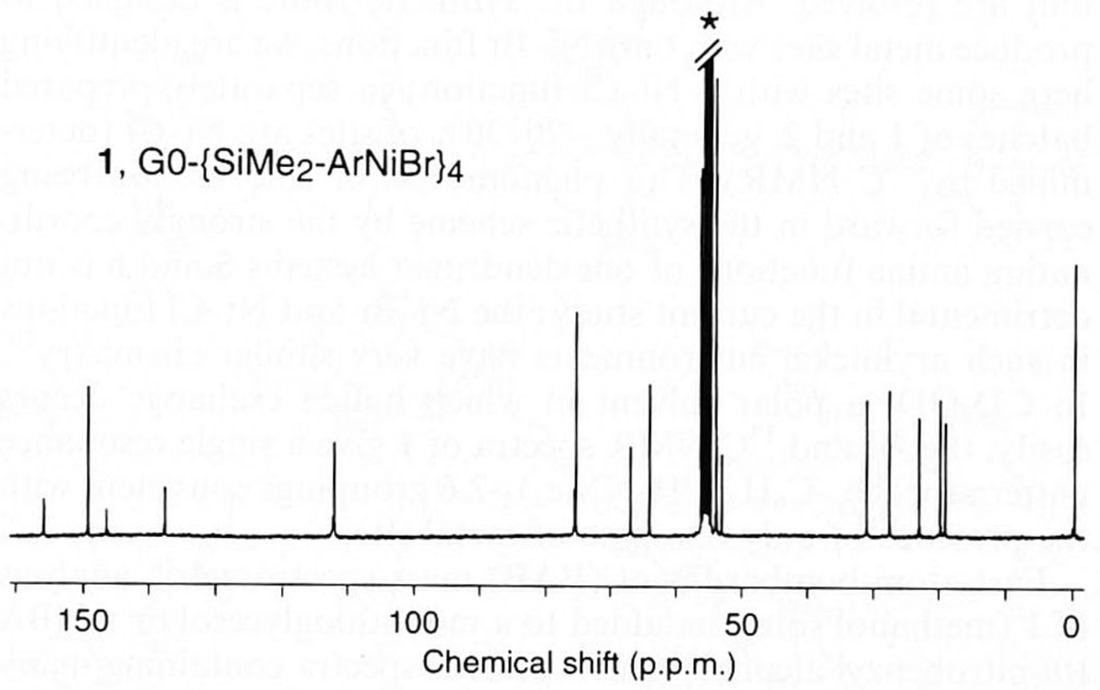


FIG. 4 75 MHz $^{13}$C NMR spectrum of dendrimer **1** in $CD_2Cl_2$ at 300 K; solvent peaks indicated by asterisk.

first-generation aryl bromide dendrimers **5** and **6** is not complicated and these compounds are now being employed as starting materials for the synthesis of other metal-containing materials with preselected (catalytic) properties that may find application in two-phase or membrane reactors. □

Received 17 August; accepted 9 November 1994.

1. Chaloner, P. A. *Handbook of Coordination Catalysis in Organic Chemistry* (Butterworth, London, 1986).
2. van de Kuil, L. A. *et al. Organometallics* **13,** 468–477 (1994).
3. van de Kuil, L. A. *et al. Chem. Mater.* **8,** 1675–1683 (1994).
4. Mekelburger, H-B., Jaworek, W. & Vögtle, F. *Angew. Chem. int. Edn. engl.* **31,** 1571–1576 (1992).

5. Tomalia, D. A., Naylor, A. M. & Goddard, W. A. *Angew. Chem. int. Edn. engl.* **29,** 138–175 (1990).
6. Tomalia, D. A. *Aldrichim. Acta* **26,** 91–101 (1993).
7. Achar, S. & Puddephatt, R. J. *Angew. Chem. int. Edn. engl.* **33,** 1493–1495 (1994).
8. Serroni, S. *et al. Angew. Chem. int. Edn. engl.* **31,** 1493–1495 (1992).
9. Moulines, F., Gloaguen, B. & Astruc, D. *Angew. Chem. int. Edn. engl.* **31,** 458–460 (1992).
10. Newkome, G. R. *et al. J. chem. Soc., chem. Commun.* 925–927 (1993).
11. Liao, Y-H. & Moss, J. R. *J. chem. Soc., chem. Commun.* 1774–1777 (1993).
12. van de Kuil, L. A. *et al. Recl Trav. chim. Pays-Bas* **113,** 267–277 (1994).
13. van der Made, A. W. & van Leeuwen, P. W. N. M. *J. chem. Soc., chem. Commun.* 1400–1401 (1992).
14. van der Made, A. W., van Leeuwen, P. W. N. M., de Wilde, J. C. & Brandes, R. A. C. *Adv. Mater.* **5,** 466–468 (1993).
15. Seyferth, D., Son, D. Y., Rheingold, A. L. & Ostrander, R. L. *Organometallics* **13,** 2682–2690 (1994).
16. Eckert, H. & Forster, B. *Angew. Chem. int. Edn. engl.* **99,** 922–923 (1987).
17. Grove, D. M., van Koten, G., Ubbels, H. J. C., Zoet, R. & Spek, A. L. *Organometallics* **3,** 1003–1009 (1984).
18. Grove, D. M. *et al. Inorg. Chem.* **27,** 2466–2473 (1988).
19. Grove, D. M., van Koten, G. & Verschuuren, A. H. M. *J. Molec. Catal.* **45,** 169–174 (1988).
20. Grove, D. M., Verschuuren, A. H. M., van Koten, G. & van Beek, J. A. M. *J. organomet. Chem.* **372,** C1–C6 (1989).

ACKNOWLEDGEMENT. We thank J. Thomas-Oates for acquiring the FAB mass spectra of **1**.

# Climate correlations between Greenland and Antarctica during the past 100,000 years

**Michael Bender*, Todd Sowers†, Mary-Lynn Dickson*, Joseph Orchardo*, Pieter Grootes‡, Paul A. Mayewski§ & Debra A. Meese‖**

* Graduate School of Oceanography, University of Rhode Island, Kingston, Rhode Island 02881, USA
† Lamont-Doherty Earth Observatory, Palisades, New York 10964, USA
‡ Department of Geological Sciences and Quaternary Research Center, University of Washington, Seattle, Washington 98105, USA
§ Glacier Research Group, Institute for the Study of Earth, Oceans and Space, University of New Hampshire, Durham, New Hampshire 03824, USA
‖ Cold Regions of Research and Engineering Laboratory, Hanover, New Hampshire 03755, USA

**THE ice cores recovered from central Greenland by the GRIP[1,2] and GISP2[3] projects record 22 interstadial (warm) events during the part of the last glaciation spanning 20–105 kyr before present. The ice core from Vostok, east Antarctica, records nine interstadials during this period[4,5]. Here we explore links between Greenland and Antarctic climate during the last glaciation using a high-resolution chronology derived by correlating oxygen isotope data for trapped $O_2$ in the GISP2 and Vostok cores. We find that interstadials occurred in east Antarctica whenever those in Greenland lasted longer than 2,000 years. Our results suggest that partial deglaciation and changes in ocean circulation are partly responsible for the climate teleconnection between Greenland and Antarctica. Ice older than 115 kyr in the GISP2 core shows rapid variations in the $\delta^{18}O$ of $O_2$ that have no counterpart in the Vostok record. The age–depth relationship, and thus the climate record, in this part of the GISP2, core appears to be significantly disturbed.**

The oxygen isotope ratio ($\delta^{18}O$) of $O_2$ in the modern atmosphere ($\delta^{18}O_{atm}$) is ~23.5‰ heavier than mean ocean water[6], mainly due to fractionation of the oxygen isotopes during photosynthesis, respiration and hydrological processes[7–9]. (See Fig. 1 legend for a definition of $\delta^{18}O$). The $\delta^{18}O$ of sea water ($\delta^{18}O_{sw}$) has varied with fluctuations in the volume of continential ice[10]. During the past 135 kyr, $\delta^{18}O_{atm}$ has followed $\delta^{18}O_{sw}$ variations because photosynthesis transmits variations in $\delta^{18}O_{sw}$ to $O_2$ in air[11,12]. Although $\delta^{18}O$ of $O_2$ varies with time, it is constant throughout the atmosphere at any one time because the turnover time of $O_2$ (~$1.2 \times 10^3$ yr)[9] is much longer than the mixing time of the atmosphere (~1 yr). Hence $\delta^{18}O$ of $O_2$ can be used to intercorrelate ice cores, and to correlate ice cores with the deep-sea sediment oxygen-isotope stratigraphy[11,12].

Sowers *et al.*[11] measured $\delta^{18}O_{atm}$ in the Vostok ice core and used the results to establish a chronology for trapped gases in that ice core which is consistent with the SPECMAP chronology (Fig. 1). We present a new record of $\delta^{18}O_{atm}$ from the GISP2 core (based on the analysis of 201 samples between 100 and 3,050 m depth) and use the results to establish a chronology which is consistent with that of Vostok[11] as well as the deep-sea sediment record (Fig. 1). Because $\delta^{18}O_{atm}$ is relatively constant between 25 and 49 kyr ago, we consider the correlations between Vostok, SPECMAP and GISP2 to be inadequate during this period, and focus our discussion on ice which is older than 49 kyr.

We derive an age–depth relationship for the GISP2 core by correcting for the fact that gases are trapped 70–90 m below the surface, making the gas younger than the surrounding ice[13,14]. Our ice-core chronologies are not necessarily the most accurate, but they provide the most precise relative ages for comparing GISP2 and Vostok climate records with one another as well as with deep-sea records in the range 50–105 kyr. We estimate the uncertainty in relative ice ages at GISP2 and Vostok as <3 kyr, half of which comes from uncertainties in correlating gas records and half from uncertainties in differences between gas and ice ages at Vostok. We also note that our absolute chronology is in excellent agreement with that derived for the GRIP core by Dansgaard *et al.*[2] based on a flow model and assigned ages for two depths in the core.

In Fig. 1, we plot $\delta D$ of Vostok ice ($\delta D_{ice}$)[5,15] and $\delta^{18}O$ of GISP2 ice ($\delta^{18}O_{ice}$)[3] against SPECMAP age. The isotopic composition of hydrogen and oxygen in precipitation reflect condensation temperatures, with heavier values corresponding to warmer temperatures. There are 22 distinct interstadial events recorded in the GISP2 (and GRIP) record between 20 and 105 kyr ago (refs 1–3). These well documented events range in duration from ~0.4 to 12 kyr (from first warming to final cooling). Eight of the nine long (>2 kyr from glacial baseline to glacial baseline) interstadial events at GISP2 can be clearly recognized in the Vostok record as increases in $\delta D$ of at least 15‰, corresponding to warmings of 2 °C or more[16,17]. The correlation of events 8 and 12 to Vostok events dated at 39 and 46 kyr is uncertain because the Vostok chronology is poorly defined in this period. Small warming events, largely buried in the noise at Vostok, may correspond to the shorter Greenland interstadials, but these events cannot be intercorrelated with confidence.

The nature of the correlated long interstadial events differs between Greenland and Antarctica. In Greenland, interstadial events (from cold baseline to cold baseline) are characterized by very rapid warming, moderate cooling during the interstadial, and then very rapid cooling at its end. At Vostok, related events are characterized by slow warmings and slow coolings. Interstadial events 21 and 23 appear to coincide between GISP2 and Vostok, but we cannot say whether Greenland or Antarctica warmed first. Other events may be in phase or out of phase given present resolution. We are impressed by the observations that climate change is more rapid, and events more numerous, in Greenland than in Antarctica. We infer that, during the last glacial period, interstadials began in the Northern Hemisphere and subsequently spread to Antarctica if they lasted long enough. However, this inference cannot yet be proven. Furthermore, the nature of interstadial forcing and response may vary from one event to the next.

A number of factors may be responsible for the interstadial events observed in Greenland and Antarctica, and their approximate synchrony. Insolation is the first factor, especially because orbital frequencies have been identified in both the Vostok and Greenland temperature records[2,18]. Interstadials 21 and 23 fall within marine isotope substages 5a and 5c, respectively, and